Physica Medica 103 (2022) 157–165

Contents lists available at ScienceDirect

Physica Medica

journal homepage: www.elsevier.com/locate/ejmp

Technical note

Evaluation of CBCT based dose calculation in the thorax and pelvis using two generic algorithms

R.S. Thing [a,b,*], R. Nilsson [c], S. Andersson [c], M. Berg [a,b], M.D. Lund [a]

[a] Department of Oncology, Vejle Hospital, University Hospital of Southern Denmark, Beriderbakken 4, Vejle, DK-7100, Denmark
[b] Radiotherapy Research Team, Vejle Hospital, University Hospital of Southern Denmark, Beriderbakken 4, Vejle, DK-7100, Denmark
[c] RaySearch Laboratories, Stockholm, SE-103 65, Sweden

ARTICLE INFO

Keywords:
Cone beam CT
Artefact correction
Deformable image registration
Adaptive radiotherapy

ABSTRACT

Purpose: This work examines the dosimetric performance of two algorithms creating a corrected CBCT (corrCBCT) and a virtual CT (vCT) implemented in a commercial treatment planning system.
Methods: 60 patients distributed across all patient groups treated with curative intent at Vejle Hospital (breast, lung, prostate and anal/rectal cancer) were selected for the present study. Clinical treatment plans were recalculated on corrCBCT and vCT, as well as a reference CT (refCT) acquired as close in time to the CBCT image as possible. Recalculated doses were compared using gamma analysis, as well as by comparing $D_{98\%}$, $D_{50\%}$, and $D_{2\%}$ for all delineated targets and organs at risk.
Results: High dosimetric accuracy is demonstrated on both the corrCBCT and vCT. Gamma 2%/2 mm pass rates >98% were found for all patients except two outliers still having >93% pass rates. Equivalence of all evaluated dose metrics within ±1 Gy was observed for all patient groups, while the pelvic patients additionally showed equivalence for all metrics within ±1% of the refCT dose. For the thoracic patients, equivalence within ±2.5% was established for all metrics except median dose to the ipsilateral lung, calculated on corrCBCT for the breast patient group.
Conclusion: The corrCBCT and vCT images are shown in excellent dosimetric agreement with refCT images, and show high potential for future use for streamlined adaptive radiotherapy workflows.

1. Introduction

Pre-treatment Cone Beam Computed Tomography (CBCT) images are routinely used for daily verification and correction of the patient treatment position prior to delivery of a radiotherapy treatment fraction. When anatomical changes of a certain severity is observed on these images, an adaptive radiotherapy (ART) workflow will often be initiated [1,2]. The first step of the ART workflow is to determine if the observed changes are sufficient to require treatment plan adaptation. This can be estimated in various ways, and if the pre-treatment CBCT images can be used for direct dose calculation, it is easy to assess the dosimetric consequences of the observed anatomical changes. Unfortunately, clinical CBCT image quality is degraded from artefacts, arising from scattered radiation [3–5], detector lag/ghosting [6], beam hardening [7] and several other effects [8]. Therefore, additional CT scanning of the patient is often required to determine if treatment plan adaptation is indicated, causing additional patient discomfort and possibly delaying the actual adaptation of the treatment plan.

Several methods have been proposed to allow dose to be calculated directly on the CBCT images acquired for image guided radiotherapy (IGRT) on conventional linacs. These methods range from site- or patient specific CBCT calibration [9–12], deformable image registration (DIR) of the planning CT to the daily CBCT [13–15], bulk density override of tissues in the CBCT image [16], physics-based artefact corrections [17], histogram matching [18] and deep learning methods [19–21]. A comprehensive review of the different approaches and associated dose calculation accuracy was recently published by Giacometti et al. [22]. While many methods have demonstrated high accuracy for dose calculations, a widespread adoption of such methods for routine ART is not yet observed.

In recent years, dedicated treatment machines for online plan adaptation have emerged. These are either based on MRI [23–25], CBCT [26,27] or megavoltage CT [28] images, and the key difference between offline and online ART seems to be in the integration of the treatment plan evaluation, recalculation and adaptation with the treatment delivery system. The online adaptive process obviously

* Corresponding author at: Department of Oncology, Vejle Hospital, University Hospital of Southern Denmark, Beriderbakken 4, Vejle, DK-7100, Denmark.
E-mail address: rune.slot.thing@rsyd.dk (R.S. Thing).

https://doi.org/10.1016/j.ejmp.2022.10.012
Received 2 March 2022; Received in revised form 26 September 2022; Accepted 22 October 2022
Available online 31 October 2022

Table 1
CT acquisition protocols used on the Siemens Somatom Definition AS scanner. CARE Dose 4D is the automatic exposure control system on the Siemens scanner [33]. All lung patients were scanned using phase-binned 4D CT, with the Anzai Respiratory Gating Load cell system for respiratory monitoring (Anzai Medical Co. Ltd, Tokyo, Japan).

Site	kVp	mAs	Slice thickness [mm]	Pitch [mm]
Breast	120	CARE Dose 4D	0.6	1.2
Lung	120	40 per revolution	0.6	0.09
Pelvis	120	CARE Dose 4D	0.6	0.6

requires more time to complete than delivery of a regular treatment fraction on a conventional linac, and the therapeutic gain of online ART remains to be established for various patient groups [29]. While highly moveable and deformable targets may indeed benefit from online ART on a dedicated machine, anatomical changes that remain stable for hours or days may be treated sufficiently accurate with offline ART. The key benefit of offline ART is that it does not increase the treatment delivery time, which allows clinics to retain a high patient throughput. Furthermore, offline ART can be realized on conventional linacs if the pre-treatment CBCT images can be used for plan recalculation and adaptation.

This work evaluates the dosimetric performance of two algorithms for post-processing of clinical CBCT images, implemented in a commercial treatment planning system (TPS), and applied to CBCT images of patients in all groups treated with curative intent at Vejle Hospital. The algorithms are independent of specific calibrations of the CBCT images before or during acquisition, and designed to work across CBCT acquisition systems.

2. Methods

2.1. Patient groups and clinical imaging

60 patients were identified, who had all consented to their imaging and treatment plan data being used for development of new treatment strategies (Region of Southern Denmark study number 19/4307). 40 patients were distributed with 10 patients in each group of patients treated with curative intent at Vejle Hospital: breast, lung, prostate and anal/rectal cancer. These patients all had their clinical treatment plans optimized on conventional CT-images acquired on a Siemens Somatom Definition AS CT VA48A (Siemens Healthcare GmbH, Erlangen, Germany) with 2.5 mm reconstructed slice thickness. CT protocol details are provided in Table 1. An additional 20 patients treated in an MR-only workflow were included, 10 prostate and 10 anal/rectal patients. Treatment plans for these patients were optimized on MR-derived synthetic CTs (MRCAT Pelvis; RTgo v4.0) [30–32], acquired on a Philips Ingenia MR-RT scanner with 1.15 mm slice thickness (Philips Medical Systems, Eindhoven, The Netherlands). Dose prescriptions for all 60 patients are listed in Table 2.

To minimize anatomical differences between CT and CBCT images used for dose calculation, priority was given to patients who had received a rescanning CT (rCT) (n = 21, see Table 2 for distribution among patient groups.). For these patients, CBCT images from the same day as the rCT were extracted. For the remaining 39 patients, the first fraction CBCT was used, after ensuring that no major anatomical changes had occurred between pCT and first fraction CBCT acquisition. All CBCT images were acquired using the Elekta XVI r5.0.4 system (Elekta Ltd., Crawley, UK). An overview of the used CBCT scanning protocols is provided in Table 3. All CBCT images were exported to DICOM in full clinical resolution ($1 \times 1 \times 1\ mm^3$) in the treated position, using an in-house built Matlab function.

The clinical CBCT to CT match was performed according to our clinical guidelines. Breast patients were soft tissue matched on the delineated targets, retracted from the surface of the patient. Lung patients were soft tissue matched to a single match target, while other targets have larger PTV-margins to account for the increased uncertainty in daily positioning. Prostate patients were matched on gold seeds in the prostate, and anal/rectal patients were matched on bony anatomy in the pelvis. All patient corrections to the treatment position were applied as translations only.

2.2. Treatment plan recalculation

Clinical treatment plans were optimized in RayStation version 6A, 8A or 10B (RaySearch Laboratories AB, Stockholm, Sweden), with treatments delivered on beam matched Elekta Synergy, Infinity or VersaHD linacs (Elekta Ltd., Crawley, UK). Nine breast patients were treated with 3D-conformal technique using a mix of 6 and 18 MV photon beams, while the remaining 51 patients were treated with 6 MV volumetric arc therapy (VMAT). The prescribed dose ranged from 1.8 Gy to 2.67 Gy per fraction for all patients with the majority receiving 2 Gy per fraction. Plan recalculation was performed in a research build of RayStation (version 10.1.110.51), and dose was calculated using Collapsed Cone version 5.4 in RayStation. Dose grid resolution for all plans was $2.5 \times 2.5 \times 2.5\ mm^3$.

From the clinical CT and CBCT images, three different image sets were created for dose calculation: A *corrected CBCT* (corrCBCT), a *virtual CT* (vCT), and a *reference CT* (refCT). All image sets were created from clinical images in the research version of RayStation. All DIRs described in the following were created with the ANACONDA algorithm [36], using a resolution of $5 \times 5 \times 5\ mm^3$ and a so-called Focus ROI retracted 3 cm from the edge of the CBCT field-of-view (FOV) to avoid edge effects in the DIR. Examples of the same slice of a patients pCT, clinical CBCT, corrCBCT and vCT images are shown in Fig. 1.

A schematic overview of the processing involved in the creation of each image set is shown in Fig. 2. Clinical CBCT images were imported manually into the TPS, and all following steps were scripted to demonstrate that the process can be automated, as well as to ensure reproducible image creation and plan evaluation. Script run time, including DIR, image generation of corrCBCT and vCT, dose calculation, and export of evaluation doses to file, was less than 3 min for each patient. In particular, generation of the corrCBCT and vCT was completed in around 10 s per image.

2.3. Corrected CBCT (corrCBCT)

The corrCBCT images are created through an iterative two-step process, where the planning CT (pCT) is first aligned to the CBCT anatomy using DIR. A scan-specific calibration of the CBCT image intensities is then achieved from a two dimensional histogram by identifying peak intensities corresponding to same-type tissues found in the CBCT and pCT. This calibration results in a piecewise linear conversion function applied to the CBCT grey values to make the CBCT values similar to the pCT HU.

The conversion function allows quantitative comparison of the CBCT and pCT images. The difference between the images is used to estimate an artefact correction map for the CBCT focusing on low frequency variations found in the CBCT image, but not present in the pCT. The image difference is masked to avoid residual anatomical differences from influencing the correction. The image conversion and artefact correction steps are iteratively performed, where the improvement of one step improves the other, until convergence. For the subsequent dose calculation, the corrCBCT uses the same HU to density curve as the pCT image.

In case the patient anatomy extends beyond the CBCT FOV, image information from the deformed pCT can be stitched to the corrCBCT images outside the CBCT FOV. An example of this stitching is shown in Fig. 1(c).

The algorithm creating the corrCBCT is a further development of the method first described in Thummerer et al. [37] as the *Analytical image-based correction method*.

Table 2
Characteristics of dose and fractionation for all patients in the present study. LN denotes Lymph Node targets. Treatments were prescribed according to Danish national guidelines, if not stated otherwise in the table. The number in brackets after the patient numbers, specify how many patients in each group were rescanned.

Pt group	Dose [Gy]	# Fx	# Patients (rescan)	Comments
Breast	50	25	7 (1)	Incl. loco-regional LN
Breast	40	15	3 (0)	Breast only
Lung	66	33	10 (9)	
Prostate	78	39	9 (4) CT 9 (3) MRCAT	8 incl. elective LN All incl. elective LN
Prostate	70	35	1 (1) CT 1 (0) MRCAT	Salvage treatment
Anal	60	30	1 (1) CT	
Anal	60.2	28	3 (1) CT 4 (0) MRCAT	Incl. elective LN
Rectal	62	28	4 (1) CT 3 (0) MRCAT	WW2 protocol [34,35]
Rectal	50.4	28	2 (0) CT 3 (0) MRCAT	Incl. elective LN

Table 3
CBCT acquisition protocols used on the XVI 5.0 system. The S20 collimator corresponds to a reconstructed FOV of Ø27 cm, while M20 and L20 have Ø41 cm and Ø50 cm. The cranio-caudal extent of all scans used is 27 cm. It is noted that one breast patient was scanned using the lung preset, due to bilateral treatment which could not be visualized with the small FOV of the breast preset.

Preset	Coll	Filter	mA	ms	Frames	Rotation (IEC61217)	# Patients
Breast	S20	F0	10	10	200	153°–310° or 180.1°–23°	9
Lung	M20	F1	25	40	330	180.1°–179.9°	11
Pelvis	S20	F1	25	40	200	337°–179.9°	39
Large	L20	F1	25	32	600	180.1°–179.9°	1

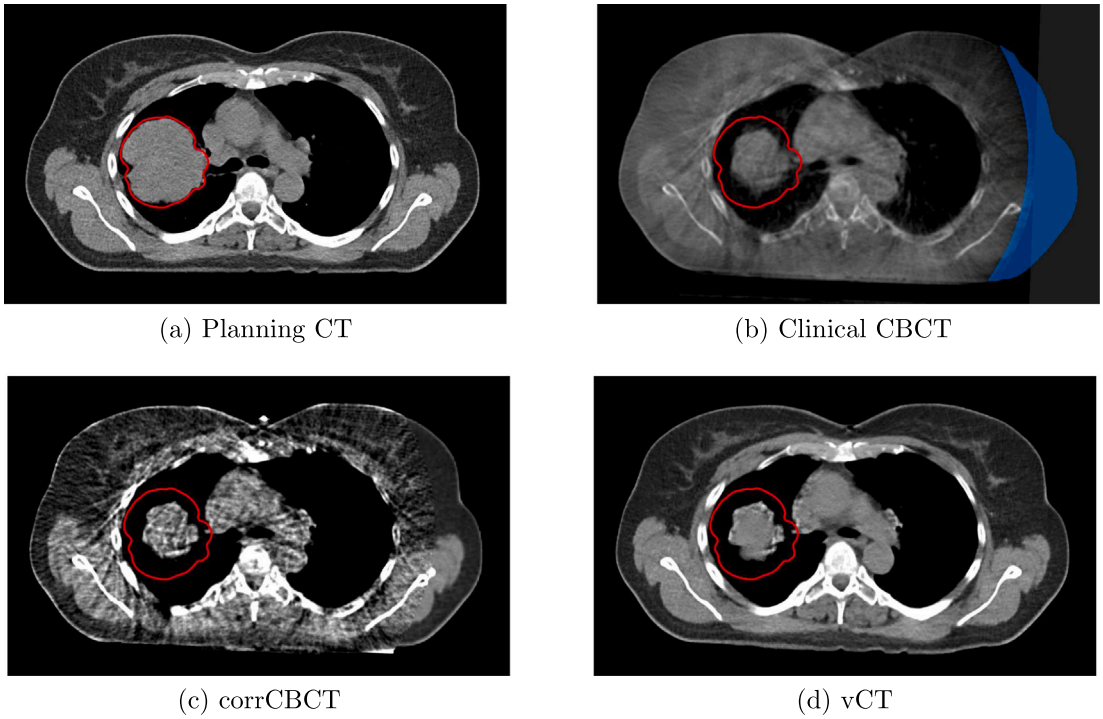

Fig. 1. Example of slices in a lung cancer patient's planning CT (a), clinical CBCT (b), corrected CBCT (corrCBCT, c) and virtual CT (vCT, d). The red tumor delineation from the planning CT is rigidly transferred to the other images, where substantial tumor shrinkage is visible in the patient's right lung. The blue area on the clinical CBCT indicates the area outside FOV which is copied from the planning CT when creating the corrCBCT and vCT images.

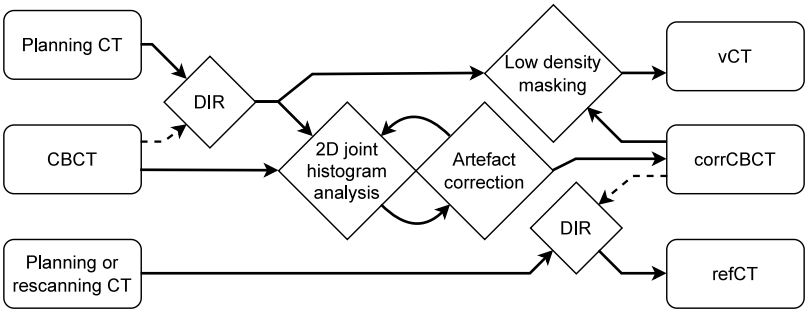

Fig. 2. Schematic overview of the image processing involved in creating the three image sets used for dose recalculation. Rectangular boxes are image sets, while diamonds are processing steps. Dashed lines indicate that an image set is used as reference in DIR.

2.4. Virtual CT (vCT)

The vCT images are designed to preserve HU values from the pCT, while using the anatomy of the clinical CBCT. This is achieved by first using a provided DIR to deform the pCT to the clinical CBCT image. Edge effects are avoided by using a Focus ROI while calculating the DIR, and a smooth transition from the CBCT anatomy to the planning CT anatomy is applied towards the boundary of the CBCT FOV.

To preserve local anatomical changes such as bowel gas, pleural effusion or other changes which manifest as large changes in density locally ($\Delta\rho > 0.3\,\mathrm{g/cm^3}$), such regions are masked automatically by the algorithm creating the vCT. Instead of using the HU from the pCT in these regions, values from the corrCBCT image is used directly. This correction is only performed where one image (pCT or clinical CBCT) has a low density region ($\rho < 0.6\,\mathrm{g/cm^3}$), to avoid duplicating bone or other high-density structures. An example of this use of the corrCBCT values is shown at the very edge of the tumor and at the boundary between lung and mediastinum in Fig. 1(d).

2.5. Reference CT (refCT)

Whenever a rCT was available, this was used as the gold standard image for the dose calculation on same day CBCT. If no rCT was available, the pCT was used instead, with the first fraction CBCT as the most similar CBCT image. DIR was performed to minimize residual anatomical variations, using the corrCBCT as reference. The deformed CT image will be referred to as the reference CT (refCT).

2.6. Dose evaluation

Dose distributions on the three image sets per patient were compared using 2%/2 mm gamma analysis with the refCT based dose as reference (gold standard). The prescribed dose was used as global reference dose, with a 10% threshold as low dose cut-off.

To compare metrics relevant for clinical evaluations in relation to ART, $D_{98\%}$, $D_{50\%}$, and $D_{2\%}$ was calculated for all target structures and organs at risk (OAR) receiving more than 0.1 Gy to 98% of the ROI volume. The target structures were rigidly copied from the pCT to the clinical CBCT image, while OAR delineations were deformably propagated to mimic a clinical workflow. No manual edits of the contours were performed in the present work. From the clinical CBCT image, all ROIs were rigidly copied to the corrCBCT, vCT and refCT image sets, to ensure that doses were compared in the same geometrical regions of the images.

Gamma analysis and dose difference calculations were performed in Matlab 2015a (MathWorks, Massachusetts, USA).

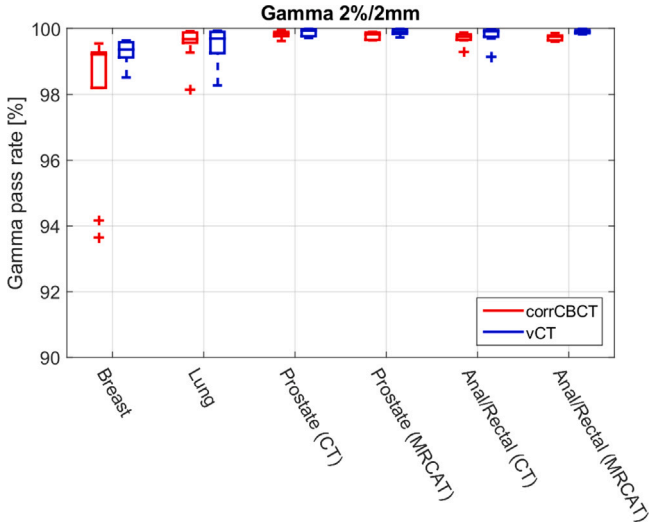

Fig. 3. Gamma 2%/2 mm pass rates for all patient groups. Pass rates for vCT images are significantly higher than for the corrCBCT for all patient groups except lung.

2.6.1. Clinical acceptance levels

To determine the clinically acceptable dose variations between the CBCT and refCT based dose calculations, we had an internal discussion between two consultant oncologists and two medical physicists at Vejle Hospital. Consensus was established at gamma 2%/2 mm pass rates above 97%, and dose metric differences of less than ±1 Gy or ±1% being fully acceptable for clinical applications.

2.7. Statistical analysis

Statistical analysis was performed in Matlab 2015a using Wilcoxon signed rank tests for paired comparisons of gamma pass rates achieved on the image sets.

The two one-sided test of equivalence for paired samples (TOST-P) was used with equivalence intervals of ±1 Gy or ±1% [38–40] to determine if the CBCT-based dose metrics are equivalent to the CT-based dose metrics. The relative dose comparison within ±1% is calculated relative to the CT-based dose metric.

Results are considered significant if $p < 0.05$.

3. Results

Plots of gamma 2%/2 mm pass rates for all patient groups are shown in Fig. 3. All pass rates were observed higher than 98%, except for two outliers in the corrCBCT of the breast group. These outliers still have pass rates above 93%. For all patients but the two breast outliers, the gamma pass rates are higher than the clinical acceptance level of 97%, and thus considered acceptable for clinical use of both algorithms.

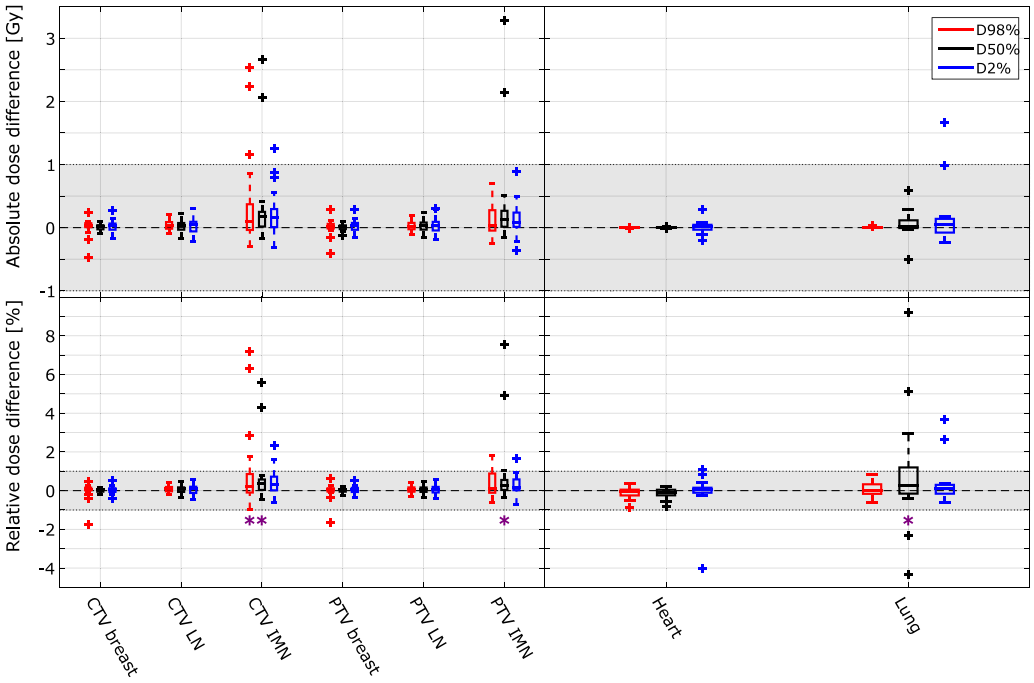

Fig. 4. Combined corrCBCT and vCT dose difference metrics for breast patients. The top row shows the absolute dose difference, while the bottom row shows relative difference. A purple asterisk indicates that the relative metrics are NOT equivalent in the TOST-P test (equivalence bounds are shown as grey area). For the target ROIs, LN denotes periclavicular lymph nodes, while IMN denotes internal mammary nodes. Breast denotes both breast and chest wall targets.

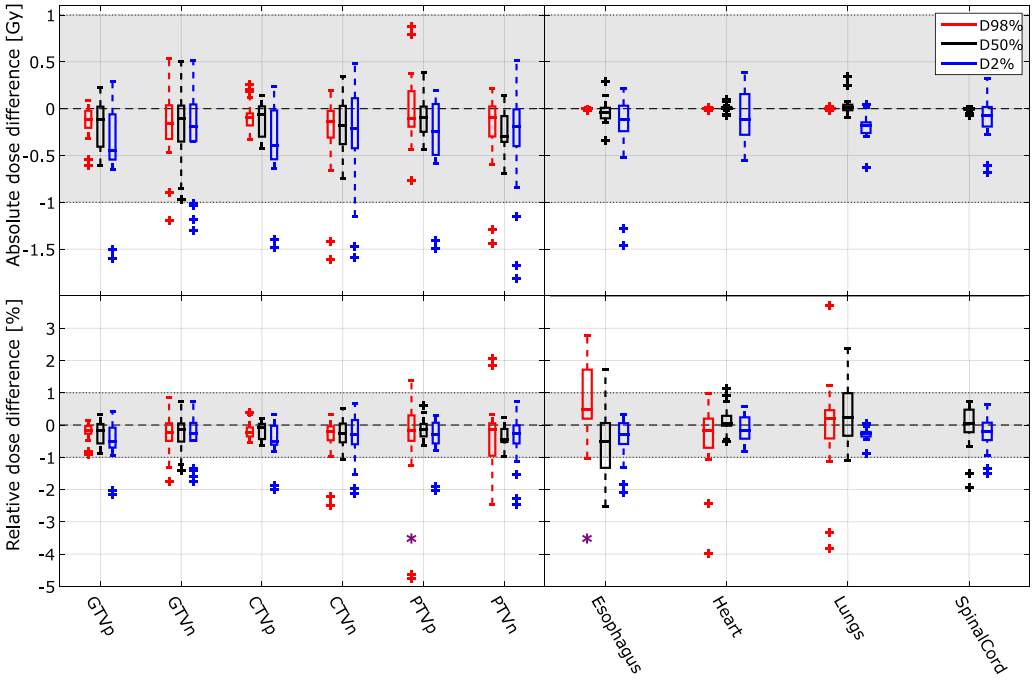

Fig. 5. Combined corrCBCT and vCT dose difference metrics for the lung patients. The top row shows the absolute dose difference, while the bottom row shows relative difference. A purple asterisk indicates that the relative metrics are NOT equivalent in the TOST-P test (equivalence bounds are shown as grey area). For targets, p denotes tumors in the lung, while n denotes nodal targets. Lungs are the sum of both lungs, excluding all GTVs. Spinal Cord $D_{98\%}$ is not shown, as doses were less than the threshold of 0.1 Gy.

Comparing the corrCBCT to vCT pass rates, the dosimetric accuracy is significantly improved on the vCT images compared to the corrCBCT, for all patient groups except lung. While statistically significant, the difference between median pass rate remains no higher than 0.2%-points for all patient groups.

Dose metric results were found highly similar across the corrCBCT and vCT images regardless of patient group. Therefore, dose difference metrics for pooled corrCBCT and vCT images are shown in Figs. 4–7. Dose metrics for the individual CBCT-based calculation methods are shown in the supplementary material, Figures S.1–S.12.

For all pelvic patients, doses are found equivalent within ±1 Gy and ±1% for all metrics considered on both the corrCBCT and vCT images. This applies both when analysing corrCBCT and vCT results alone and in pooled analysis.

In the thoracic group, all absolute dose metrics are equivalent within ±1 Gy, while several of the relative dose differences are found

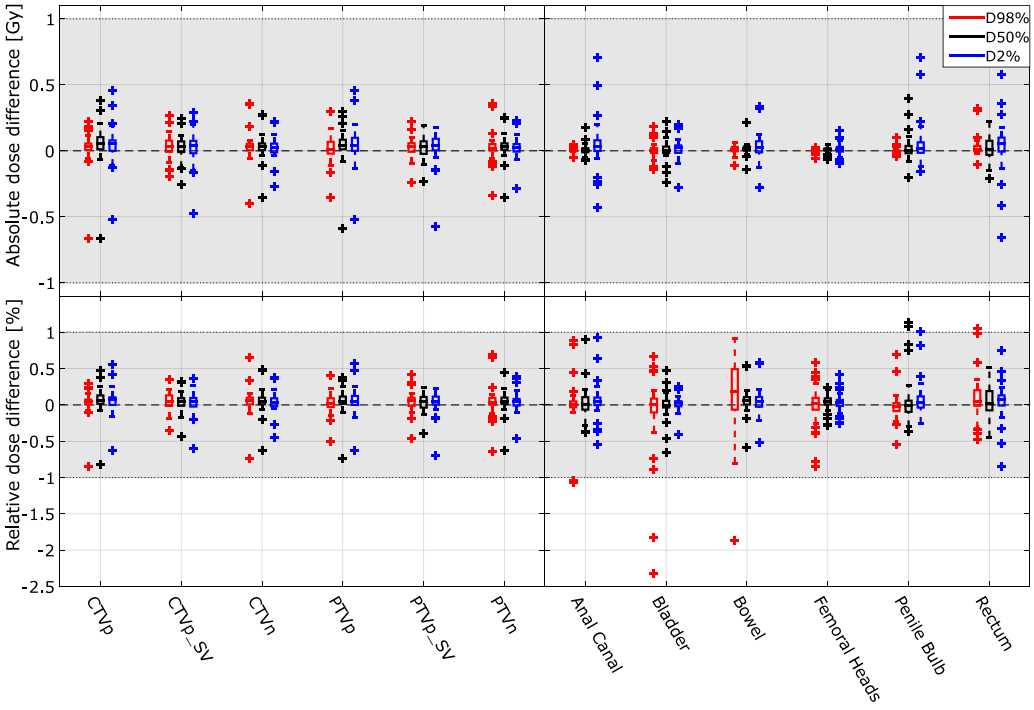

Fig. 6. Combined corrCBCT and vCT dose difference metrics for all prostate patients (CT and MRCAT). The top row shows the absolute dose difference, while the bottom row shows relative difference. All metrics are equivalent in the TOST-P test (equivalence bounds are shown as grey area). For the target ROIs, p denotes the prostate, p_SV the seminal vesicles, and n denotes the elective lymph node target.

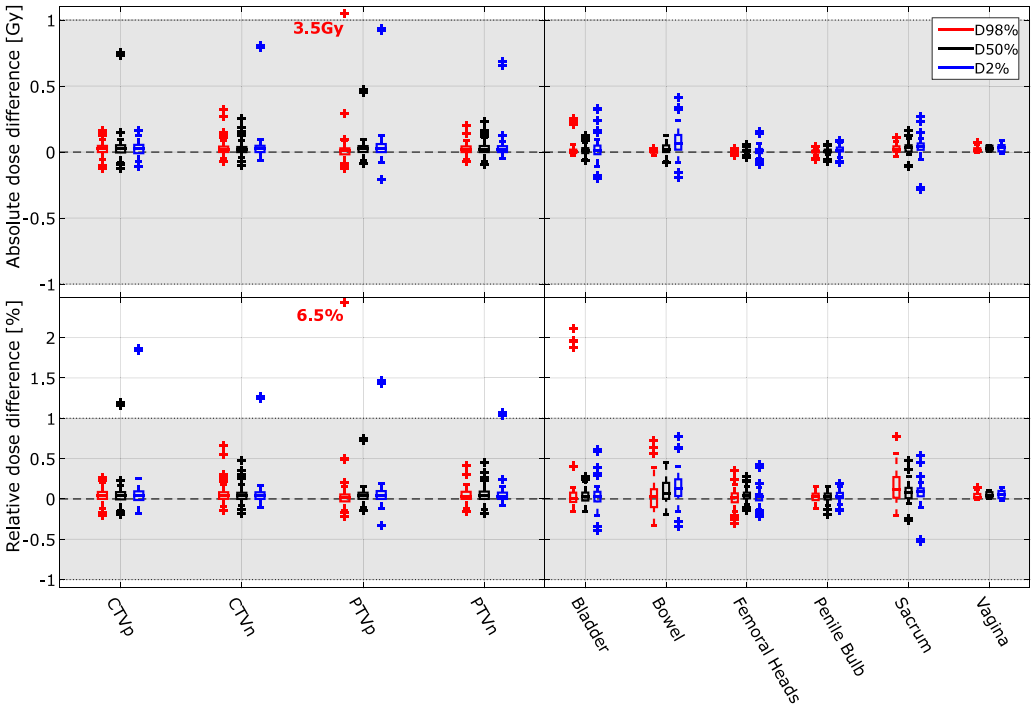

Fig. 7. Combined corrCBCT and vCT dose difference metrics for all anal/rectal patients (CT and MRCAT). The top row shows the absolute dose difference, while the bottom row shows relative difference. All metrics are equivalent in the TOST-P test (equivalence bounds are shown as grey area). For the target ROIs, p denotes the tumor and positive lymph nodes, while n denotes the elective lymph node target. Note one outlier outside the plot axis range (indicated by a marker and label).

not to be equivalent within the ±1% limit. The lack of equivalence is mainly found among ROIs located in steep dose gradients, and the median values of the dose differences remain well within the equivalence bounds.

4. Discussion

This work shows excellent dosimetric performance of the corrCBCT and vCT images for all patient groups treated with curative intent at Vejle Hospital. All gamma 2%/2 mm pass rates are above the acceptance level of 97%, except two outliers in the breast corrCBCT group. One of these outliers is due to imperfect DIR, and another due to incorrect density assignment of lung tissue. The difference in lung density translates into a too high median dose calculated to the internal mammary node target, but when looking at the dose and density distributions, the error is quite easy to identify. The outlier due to residual anatomical mismatch after DIR shows an interesting difference between the two methods, where the vCT retains a high gamma pass rate (2%/2 mm pass = 99%, as opposed to corrCBCT pass rate of 94%). With the clinical CBCT as anatomical ground truth of the daily anatomy, given that HU assignment is correct in the corrCBCT, the corrCBCT based dose calculation is likely the dose distribution closest to what the patient received on that fraction. Such a case underlines the importance of careful DIR inspection, particularly with the vCT images which may not reveal that the anatomy does not fully match the clinical CBCT.

Comparisons of dose metrics ($D_{98\%}$, $D_{50\%}$, and $D_{2\%}$) showed equivalence for all ROIs in the pelvic groups, when comparing absolute as well as relative dose differences. In the thoracic groups, all dose metrics were found equivalent within ±1 Gy, but the relative comparison revealed that not all ROI dose metrics could be considered equivalent within ±1%. In particular, challenges were observed for ROIs close to the interface between lung and soft tissue, as well as for ROIs located in steep dose gradients (i.e. the heart or esophagus). When re-testing for equivalence within ±2.5%, all ROIs were equivalent except the corrCBCT ipsilateral lung $D_{50\%}$ of the breast patients. Thus, the two methods are considered clinically acceptable for all pelvic cases, and for the thoracic patients, both algorithms are still sufficiently accurate to guide the decision for plan adaptation, when these specific limitations are kept in mind.

To illustrate the observed differences between the refCT and CBCT-based dose calculations, a worst-case breast patient is shown in Fig. 8. This particular case was a VMAT treatment plan towards the right chest wall, periclavicular and internal mammary (IMN) lymph nodes, where the left breast had previously been irradiated. To avoid overlap with previous treatment fields, a steep gradient was prioritized at the edge of the IMN target, thus leading to a treatment plan highly sensitive to anatomical variations which explains the discrepancy in dose to the IMN target. Similar worst-case examples are shown for the remaining anatomical sites in the supplementary material (Figures S.13–S.15).

Previous studies on CBCT-based dose calculation have demonstrated average gamma 2%/2 mm pass rates of 94% for thoracic patients and 98.4% for pelvic patients on CBCT images from the Varian Halcyon/Ethos system [26]. Thing et al. showed 98% pass rates or higher for lung patients scanned on the Elekta XVI system [17], and Fotina et al. have reported gamma 3%/3 mm pass rates above 98% for pelvic patients and 95% for thoracic patients [16]. The present study shows similar or improved gamma pass rates to these results. Dose metrics have been reported in additional studies, with de Smet et al. showing 2-3% difference for ROI metrics in lung patients scanned on the Elekta XVI system [41]. Kaplan et al. reported 4% dose variations on calibrated Varian OBI CBCTs [11], and this result has recently been updated to 1% dose differences for thoracic and pelvic patients [12]. This is also the case for a recent study on synthetic CT generation based on deep learning [42], where the results of this study compares or exceeds the dose calculation accuracy reported by Eckl et al.

The main drawback of the evaluated algorithms, is that both methods rely on a pCT being available for each patient (either a real or synthetic CT). On the other hand, both synthetic images can be created in about 10 s, the algorithms handle limited FOV data, and no algorithm training is required. While we only tested the corrCBCT and vCT algorithms on CBCT images from the Elekta XVI system, the methods should work on CBCTs from any system. It is well established that accurate dose calculations is more challenging on Elekta XVI images compared to Varian OBI images [41], and with the explainable algorithms, it is likely that the dosimetric performance will be at least similar for CBCT images from other systems.

The corrCBCT images may retain some low-frequency image artefacts, and streaking and image noise will not be removed by the algorithm. What the corrCBCT algorithm does provide, is images that are anatomically correct, calibrated to the HU-to-density curve of the pCT image, and where residual artefacts are visually apparent. The corrCBCT image is also robust towards large anatomical changes, as well as the quality of the DIR. Initial investigations by two of the authors (R. Nilsson and S. Andersson) show that the corrCBCT images might work well with automatic contouring algorithms, but a full clinical evaluation of the contouring accuracy on corrCBCT images has not yet been performed.

The vCT algorithm provides images with pCT-like image quality, while ensuring that low-density regions appearing or disappearing in the CBCT (compared to the pCT) are represented in the vCT as they were on the CBCT. The vCT images rely heavily on the accuracy of the DIR, and anatomical errors of the vCT compared to the underlying CBCT may be very difficult to identify. Therefore, contouring on the vCT is discouraged.

The corrCBCT and vCT images were created based on a standardized workflow, where only the DIR had to be carefully inspected — all other steps were fully scripted without individual inputs for each patient. The time required to produce the corrCBCT and vCT images and perform dose calculation on these images were no more than three minutes, from the point where a clinical CBCT image had just been imported to the TPS. We believe that the dosimetric performance and efficient workflow will allow the tools to become part of a routine workflow for ART, where all patients could have weekly (or daily) plan recalculations performed to help ensure that optimal treatment is provided. In case of anatomical changes observed on the CBCT images used for IGRT, the algorithms allow fast verification of the dose delivered, and should thus ensure that only patients who need a plan adaptation will be re-scanned. While the present study only includes 10 patients in each group investigated, the high dosimetric accuracy is promising for a full scale clinical implementation for offline dose recalculation. During clinical implementation, each case should of course be carefully inspected to ensure that eventual unexpected behaviour of the algorithms will be identified for patients differing in anatomy, target shape and location etc. from the studied cohort. Whether the corrCBCT and vCT images are suitable for manual contouring and plan re-optimization remains to be investigated.

5. Conclusion

High dosimetric accuracy of the algorithms for corrected CBCT and virtual CT implemented in RayStation have been shown for all patient groups treated with curative intent at Vejle Hospital. Both algorithms have been shown to work with traditional CT as well as MR-based synthetic CTs used for treatment planning. We consider the accuracy of both methods sufficient for clinical implementation, and we are currently planning a study to investigate if weekly CBCT-based dose calculation for all patients will change the way we perform adaptive radiotherapy in Vejle.

Acknowledgement

The research version of RayStation was provided by RaySearch Laboratories under a research agreement with Vejle Hospital. This research was supported by DCCC Radiotherapy — The Danish National Research Center for Radiotherapy, Danish Cancer Society (grant no. R191-A11526) and Danish Comprehensive Cancer Center.

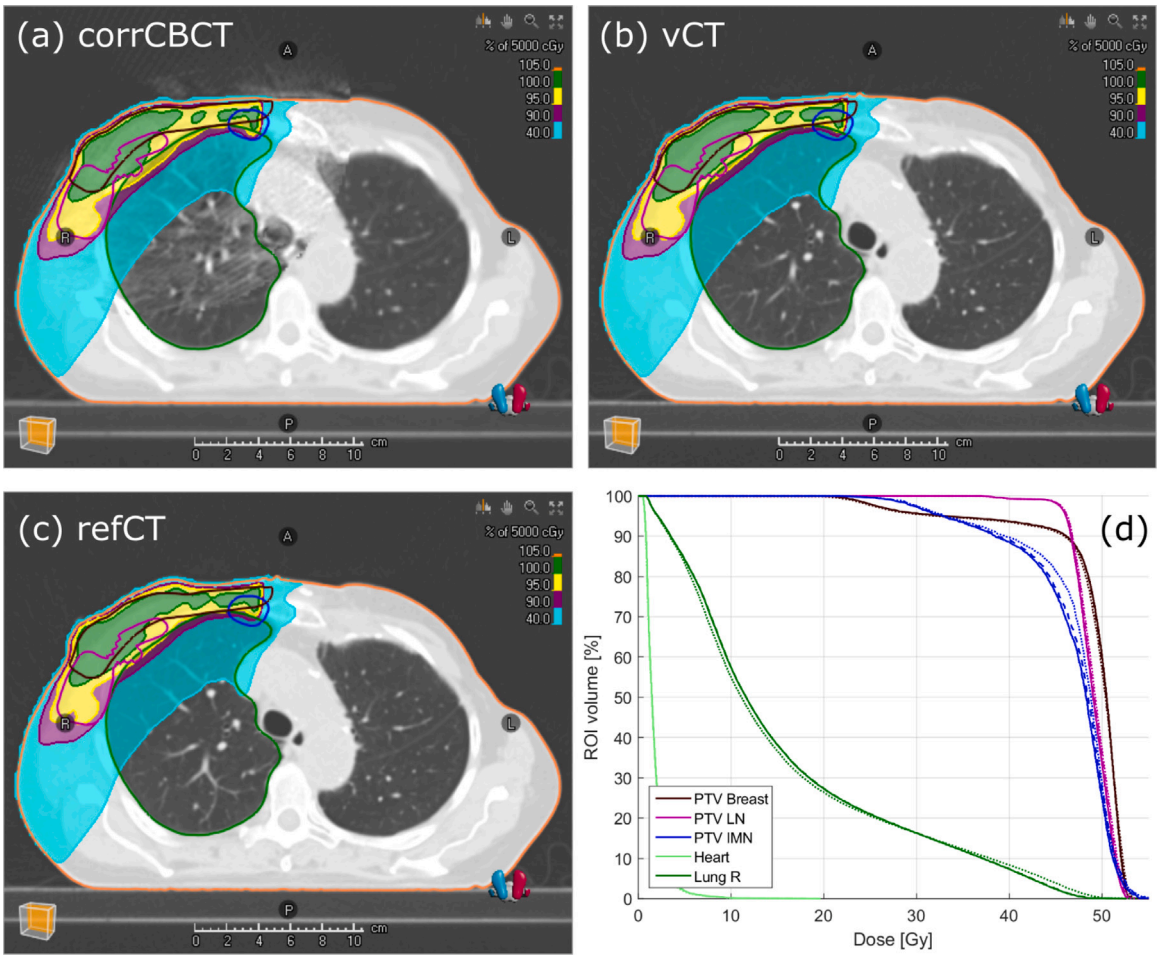

Fig. 8. Example images (a–c) and DVH curves of a breast patient, with large dose deviations to the IMN target. In the DVH curves, solid lines represent the refCT dose distributions, while dotted and dashed lines show the corrCBCT and vCT doses, respectively. CTVs have been omitted to improve readability, and the variation is similar or less than the variation of the PTV curves. ROI colours in the DVH plot matches ROI colours in the example images. Window/Level is set to 1600/-600 HU for all images.

Appendix A. Supplementary material

Supplementary material related to this article can be found online at https://doi.org/10.1016/j.ejmp.2022.10.012.

References

[1] Sonke JJ, Aznar M, Rasch C. Adaptive Radiotherapy for Anatomical Changes. Semin Radiat Oncol 2019;29(3):245–57. http://dx.doi.org/10.1016/j.semradonc.2019.02.007.

[2] Møller DS, Khalil AA, Knap MM, Hoffmann L. Adaptive radiotherapy of lung cancer patients with pleural effusion or atelectasis. Radiother Oncol 2014;110(3):517–22. http://dx.doi.org/10.1016/j.radonc.2013.10.013.

[3] Siewerdsen J, Jaffray D. Cone-beam computed tomography with a flat-panel imager: Magnitude and effects of x-ray scatter. Med Phys 2001;28(2):220–31. http://dx.doi.org/10.1118/1.1339879.

[4] Jarry J, Graham SA, Moseley DJ, Jaffray DJ, Siewerdsen JH, Verhaegen F. Characterization of scattered radiation in kV CBCT images using Monte Carlo simulations. Med Phys 2006;33(11):4320–9. http://dx.doi.org/10.1118/1.2358324.

[5] Poludniowski G, Evans PM, Kavanagh A, Webb S. Removal and effects of scatter-glare in cone-beam CT with an amorphous-silicon flat-panel detector.. Phys Med Biol 2011;56(6):1837–51. http://dx.doi.org/10.1088/0031-9155/56/6/019.

[6] Siewerdsen JH, Jaffray DA. A ghost story: spatio-temporal response characteristics of an indirect-detection flat-panel imager.. Med Phys 1999;26(8):1624–41. http://dx.doi.org/10.1118/1.598657.

[7] Herman GT. Correction for beam hardening in computed tomography. Phys Med Biol 1979;24(1):81–106. http://dx.doi.org/10.1088/0031-9155/24/1/008.

[8] Thing RS, Bernchou U, Mainegra-Hing E, Hansen O, Brink C. Hounsfield unit recovery in clinical cone beam CT images of the thorax acquired for image guided radiation therapy. Phys Med Biol 2016;61(15):5781–802. http://dx.doi.org/10.1088/0031-9155/61/15/5781.

[9] Richter A, Hu Q, Steglich D, Baier K, Wilbert J, Guckenberger M, et al. Investigation of the usability of conebeam CT data sets for dose calculation. Radiat Oncol 2008;3:42. http://dx.doi.org/10.1186/1748-717X-3-42.

[10] Elstrøm UV, Olsen SRK, Muren LP, Petersen JBB, Grau C. The impact of CBCT reconstruction and calibration for radiotherapy planning in the head and neck region - a phantom study. Acta Oncol 2014;53(8):1114–24. http://dx.doi.org/10.3109/0284186X.2014.927073.

[11] Kaplan LP, Elstrøm UV, Møller DS, Hoffmann L. Cone beam CT based dose calculation in the thorax region. Phys Imaging Radiat Oncol 2018;7(May):45–50. http://dx.doi.org/10.1016/j.phro.2018.09.001.

[12] Holm AIS, Nyeng TB, Møller DS, Assenholt MS, Hansen R, Nyvang L, et al. Density calibrated cone beam CT as a tool for adaptive radiotherapy. Acta Oncologica 2021;60(10):1275–82. http://dx.doi.org/10.1080/0284186X.2021.1945678.

[13] Onozato Y, Kadoya N, Fujita Y, Arai K, Dobashi S, Takeda K, et al. Evaluation of On-Board kV Cone Beam Computed Tomography–Based Dose Calculation With Deformable Image Registration Using Hounsfield Unit Modifications. Int J Radiation Oncol Biol Phys 2014;89(2):416–23. http://dx.doi.org/10.1016/j.ijrobp.2014.02.007.

[14] Veiga C, Janssens G, Teng C-L, Baudier T, Hotoiu L, McClelland JR, et al. First clinical investigation of cone beam computed tomography and deformable registration for adaptive proton therapy for Lung cancer. IJROBP 2016;95(1):549–59. http://dx.doi.org/10.1016/j.ijrobp.2016.01.055.

[15] Marchant TE, Joshi KD, Moore CJ. Accuracy of radiotherapy dose calculations based on cone-beam CT: comparison of deformable registration and image correction based methods. Phys Med Biol 2018;63(6):065003. http://dx.doi.org/10.1088/1361-6560/aab0f0.

[16] Fotina I, Hopfgartner J, Stock M, Steininger T, Lütgendorf-Caucig C, Georg D. Feasibility of CBCT-based dose calculation: Comparative analysis of HU adjustment techniques. Radiother Oncol 2012;104(2):249–56. http://dx.doi.org/10.1016/j.radonc.2012.06.007.

[17] Thing RS, Bernchou U, Hansen O, Brink C. Accuracy of dose calculation based on artefact corrected Cone Beam CT images of lung cancer patients. Phys Imaging Radiat Oncol 2017;1:6–11. http://dx.doi.org/10.1016/j.phro.2016.11.001.

[18] Kidar HS, Azizi H. Enhancement of Hounsfield unit distribution in cone-beam CT images for adaptive radiation therapy: Evaluation of a hybrid correction approach. Phys Med 2020;69:269–74. http://dx.doi.org/10.1016/j.ejmp.2020.01.002.

[19] Hansen DC, Landry G, Kamp F, Li M, Belka C, Parodi K, et al. ScatterNet: A convolutional neural network for cone-beam CT intensity correction. Med Phys 2018;45(11):4916–26. http://dx.doi.org/10.1002/mp.13175.

[20] Rossi M, Cerveri P. Comparison of Supervised and Unsupervised Approaches for the Generation of Synthetic CT from Cone-Beam CT. Diagnostics 2021;11(8). http://dx.doi.org/10.3390/diagnostics11081435.

[21] Spadea MF, Maspero M, Zaffino P, Seco J. Deep learning based synthetic-CT generation in radiotherapy and PET: A review. Med Phys 2021;48(11):6537–66. http://dx.doi.org/10.1002/mp.15150.

[22] Giacometti V, Hounsell AR, McGarry CK. A review of dose calculation approaches with cone beam CT in photon and proton therapy. Phys Med 2020;76:243–76. http://dx.doi.org/10.1016/j.ejmp.2020.06.017.

[23] Mutic S, Dempsey JF. The ViewRay System: Magnetic Resonance–Guided and Controlled Radiotherapy. Semin Radiat Oncol 2014;24(3):196–9. http://dx.doi.org/10.1016/j.semradonc.2014.02.008.

[24] Liney G, Whelan B, Oborn B, Barton M, Keall P. MRI-linear accelerator radiotherapy systems. Clin Oncol 2018;30(11):686–91. http://dx.doi.org/10.1016/j.clon.2018.08.003.

[25] Winkel D, Bol GH, Kroon PS, van Asselen B, Hackett SS, Werensteijn-Honingh AM, et al. Adaptive radiotherapy: The Elekta Unity MR-linac concept. Clin Transl Radiat Oncol 2019;18:54–9. http://dx.doi.org/10.1016/j.ctro.2019.04.001.

[26] Hu Y, Arnesen M, Aland T. Characterization of an advanced cone beam CT (CBCT) reconstruction algorithm used for dose calculation on Varian Halcyon linear accelerators. Biomed Phys Eng Express 2022;8(2):025023. http://dx.doi.org/10.1088/2057-1976/ac536b.

[27] Tegtmeier RC, Ferris WS, Bayouth JE, Miller JR, Culberson WS. Characterization of imaging performance of a novel helical kVCT for use in image-guided and adaptive radiotherapy. J Appl Clin Med Phys 2022;23(6):e13648. http://dx.doi.org/10.1002/acm2.13648.

[28] Langen KM, Meeks SL, Poole DO, Wagner TH, Willoughby TR, Kupelian PA, et al. The use of megavoltage CT (MVCT) images for dose recomputations. Phys Med Biol 2005;50(18):4259–76. http://dx.doi.org/10.1088/0031-9155/50/18/002.

[29] Lim-Reinders S, Keller BM, Al-Ward S, Sahgal A, Kim A. Online adaptive radiation therapy. IJROBP 2017;99(4):994–1003. http://dx.doi.org/10.1016/j.ijrobp.2017.04.023.

[30] Maspero M, Seevinck PR, Schubert G, Hoesl MA, Van Asselen B, Viergever MA, et al. Quantification of confounding factors in MRI-based dose calculations as applied to prostate IMRT. Phys Med Biol 2017;62(3):948–65. http://dx.doi.org/10.1088/1361-6560/aa4fe7.

[31] Kemppainen R, Suilamo S, Tuokkola T, Lindholm P, Deppe MH, Keyriläinen J. Magnetic resonance-only simulation and dose calculation in external beam radiation therapy: a feasibility study for pelvic cancers. Acta Oncol 2017;56(6):792–8. http://dx.doi.org/10.1080/0284186X.2017.1293290.

[32] Christiansen RL, Jensen HR, Brink C. Magnetic resonance only workflow and validation of dose calculations for radiotherapy of prostate cancer. Acta Oncol 2017;56(6):787–91. http://dx.doi.org/10.1080/0284186X.2017.1290275.

[33] Söderberg M. Overview, practicaltips and potential pitfalls of using automatic exposure control in CT: siemens CARE dose 4D. Radiat Prot Dosim 2015;169. http://dx.doi.org/10.1093/rpd/ncv459.

[34] Hospital V. Curative chemoradiation of low rectal cancer (WW2). 2022, ClinicalTrials.gov [Internet]. Bethesda (MD): National Library of Medicine (US). 2000-2016, URL https://www.clinicaltrials.gov/ct2/show/NCT02438839.

[35] Jensen L, Poulsen L, Risum S, Nielsen J, Mynster T, Pløen J, et al. 400Mo curative chemoradiation for low rectal cancer: Early clinical outcomes from a multicentre phase II trial. Ann Oncol 2020;31:S411. http://dx.doi.org/10.1016/j.annonc.2020.08.511.

[36] Weistrand O, Svensson S. The ANACONDA algorithm for deformable image registration in radiotherapy. Med Phys 2015;42(1):40–53. http://dx.doi.org/10.1118/1.4894702.

[37] Thummerer A, Zaffino P, Meijers A, Marmitt GG, Seco J, Steenbakkers RJ, et al. Comparison of CBCT based synthetic CT methods suitable for proton dose calculations in adaptive proton therapy. Phys Med Biol 2020;65(9). http://dx.doi.org/10.1088/1361-6560/ab7d54.

[38] Jones B, Jarvis P, Lewis JA, Ebbutt AF. Trials to assess equivalence: the importance of rigorous methods. BMJ 1996;313(7048):36–9. http://dx.doi.org/10.1136/bmj.313.7048.36.

[39] Mara CA, Cribbie RA. Paired-samples tests of equivalence. Comm Statist Simulation Comput 2012;41(10):1928–43. http://dx.doi.org/10.1080/03610918.2011.626545.

[40] Cusumano D, Lenkowicz J, Votta C, Boldrini L, Placidi L, Catucci F, et al. A deep learning approach to generate synthetic CT in low field MR-guided adaptive radiotherapy for abdominal and pelvic cases. Radiother Oncol 2020;153:205–12. http://dx.doi.org/10.1016/j.radonc.2020.10.018.

[41] De Smet M, Schuring D, Nijsten S, Verhaegen F. Accuracy of dose calculations on kV cone beam CT images of lung cancer patients. Med Phys 2016;43(11):5934–41. http://dx.doi.org/10.1118/1.4964455.

[42] Eckl M, Hoppen L, Sarria GR, Boda-Heggemann J, Simeonova-Chergou A, Steil V, et al. Evaluation of a cycle-generative adversarial network-based cone-beam CT to synthetic CT conversion algorithm for adaptive radiation therapy. Phys Med 2020;80:308–16. http://dx.doi.org/10.1016/j.ejmp.2020.11.007.